CanX–4 and CanX–5 Precision Formation Flight: Mission Accomplished!

Grant Bonin, Niels Roth, Scott Armitage, Josh Newman, Ben Risi, Robert E. Zee
Space Flight Laboratory, University of Toronto Institute for Aerospace Studies
4925 Dufferin Street, Toronto, Ontario, Canada, M3H 5T6; +1-416-667-7873
gbonin@utias-sfl.net

ABSTRACT

In November 2014, only four months following launch, the CanX–4 and CanX–5 dual-spacecraft formation-flying mission achieved what has never been accomplished before, and successfully completed all of its mission goals with unprecedented precision and speed. This achievement—a series of autonomous formations with sub-metre control and centimetre-level relative position knowledge at the nanosatellite scale—was preceded by a rapid commissioning phase and orbit acquisition manoeuvres, which brought the two satellites from a maximum range of 2300 km to a closest controlled range of 50 m during formation flight.

Launched on 30 June 2014 from Sriharikota, India on board the Polar Satellite Launch Vehicle (PSLV), CanX–4 and CanX–5 were deployed separately following launch, after which a series of drift recovery manoeuvres were executed to bring the spacecraft within communications range of each other. Subsequently, the spacecraft used onboard propulsion, an S-band intersatellite communications link, and relative navigation using carrier-phase differential GPS techniques to perform a series of precise, controlled, autonomous formations from 1 km range down to 50 m separation. The achievements of CanX–4 and CanX–5 have set the high mark for small satellite formation flight, and the technologies and algorithms developed for this mission enable a number of future applications, from on-orbit inspection and repair to sparse aperture sensing, interferometry, and ground-moving target indication.

This paper describes the CanX–4 and CanX–5 mission and its exciting results, with an emphasis on launch, commissioning, relative orbit acquisition and phasing, and autonomous formation flight.

INTRODUCTION

The use of multiple autonomously coordinated spacecraft, often—though not necessarily—in close proximity to one another, is a critical capability to the future of spaceflight. Formation flight applications range from synthetic aperture radar and optical interferometry, to on-orbit servicing of other spacecraft, to gravitational and magnetic field science. Groups of small, relatively simple spacecraft can also potentially replace single large and complex ones, reducing risk through distribution of instruments, and cost by leveraging non-recurring engineering costs. Performance of the entire formation can be gradually built up over several launches, maintained over time with replacement units when others fail, or allowed to degrade gracefully.

The benefits of formation flight are best realized as the size of spacecraft decreases, nanosatellites being the foremost example. These spacecraft are cost-effective, easily mass-produced, and capable of being deployed en masse from a single launch. Nanosatellite technology has already matured to the point where this is possible. However, there had been no successful demonstrations of formation flight with spacecraft of this scale prior to CanX–4 and CanX–5. With their success, CanX–4&5 have paved the way for these miniaturized technologies to be integrated on spacecraft of all scales.

Formation Flight Background

Early in both the United States and the Soviet Union space programs, it was recognized that the ability to operate spacecraft in close proximity to one another would become increasingly important in order to facilitate the rendezvous of vehicles for the purposes of crew and material transfer. The first attempt at coordinated spacecraft operation was the Soviet Vostok 3 and 4 mission launched in 1962. These spacecraft were launched a day apart into nearly identical orbits, with an initial distance of about 6.5 km. Given their lack of manoeuvring thrusters, this distance quickly grew to nearly 3000 km after a few days.[1]

In 1965, in preparation for the Apollo missions where docking the lunar and command modules would be a critical mission step, US astronaut Wally Schirra successfully manoeuvred his Gemini 6 spacecraft as close as 0.3 m from the Gemini 7 spacecraft and kept station around its target at ranges up to 90 m, including a 20 minute period where no control thrusts were performed at all.[2]

More recently, advances in onboard computing capability has allowed for automated spacecraft rendezvous and docking down to the small satellite scale. The Swedish-led Prototype Research Instruments and Space Mission technology Advancement (PRISMA) mission, launched on 15 June 2010, was designed to demonstrate autonomous homing, rendezvous, formation flight, and other proximity operations, amongst other things. The space segment is composed of a main and target spacecraft, with a mass of 145 kg and 50 kg, respectively.[3] The PRISMA mission cost an order of magnitude more than CanX–4&5 to develop.[4]

Work towards autonomous formation flight of nanosatellites has been ongoing at the Space Flight Laboratory (SFL) for several years. This work can be traced back to the CanX–2 spacecraft, launched in 2008, which demonstrated a number of technologies required for formation flight, including a cold-gas propulsion system and precision GPS receiver, in a 3U form factor.[5] CanX–4 and CanX–5 represent the latest efforts in the field, and have set the bar for the state-of-the-art in nanosatellite formation flying[6] with the completion of their primary mission in November 2014.

MISSION OVERVIEW

The primary goal of the CanX–4&5 mission was to demonstrate relative position control accuracy better than one metre, 2σ, for a duration of at least 10 orbits per formation in four formations: a 1000 m along-track orbit (ATO), a 500 m ATO, a 100 m projected-circular orbit (PCO) and a 50 m PCO. The ATO can be thought of as a "leader-follower" configuration, whereby one spacecraft maintains a fixed relative separation from the other in the same orbital plane. The PCO is so named because, when viewed from Earth, one spacecraft appears to draw a circle around the other over the course of one orbit. Formation control was accomplished using one actively orbit-controlled spacecraft, designated the Deputy, and one uncontrolled spacecraft, designated the Chief.

The reference trajectories were periodic solutions to the Hill-Clohessy-Wiltshire (HCW) equations, which describe relative satellite motion assuming a circular Chief orbit and close relative separation between the spacecraft as compared to the orbit radius. These reference trajectories are given by[7]

$$\begin{aligned} x(t) &= \tfrac{1}{2} d_1 \sin(nt + \alpha), \\ y(t) &= d_1 \cos(nt + \alpha) + d_3, \text{ and} \\ z(t) &= d_2 \sin(nt + \beta), \end{aligned} \quad (1)$$

where n is the mean orbital angular velocity of the Chief spacecraft and d_1, d_2, d_3, α, and β are the formation design parameters. These solutions are expressed in the rotating local-vertical local-horizontal (LVLH) reference frame of the Chief. The *x*-axis of the LVLH frame is aligned with the position vector, while the *z*-axis is aligned with the orbital angular momentum vector, and the *y*-axis completes the orthonormal triad such that it is nominally aligned with the velocity vector. These directions are often referred to as radial, cross-track, and along-track, respectively. It is important to note that the cross-track motion is decoupled from the other components and its phase with respect to the radial motion can be adjusted to provide passively safe relative orbits, where at least one component is guaranteed to be non-zero.

Table 1: Formation design parameters

Formation	d_1 [m]	d_2 [m]	d_3 [m]	α [rad]	β [rad]	Duration [orbits]
ATO 1000	60	30	1000	0	π/2	11
ATO 500	60	30	500	0	π/2	11
PCO 100	100	100	0	0	0	11
PCO 50	50	50	0	3π/2	3π/2	11

The design parameters for the four target formations are given in Table 1. For the ATOs, a passively safe relative separation of 30 m in the radial and cross-track directions was selected to safeguard against collisions in the event of unexpected formation control loss. The PCOs could not be made passively safe since this formation required both phase angles to be equal. The phase angles for the PCOs were selected to minimize fuel during the formation reconfiguration manoeuvres. The duration of 11 orbits was selected so that fine formation control could be maintained for a full 10 orbits, allowing one orbit for convergence.

SYSTEM OVERVIEW

The CanX–4&5 spacecraft are each approximately 6 kg nanosatellites based on the SFL Generic Nanosatellite Bus (GNB) architecture. The GNB structure is a 20 cm cube, designed to interface with the SFL XPOD launch vehicle deployment system. The GNB platform (Figure 1) was designed with mission flexibility in mind. It is the basis for several existing and upcoming missions. In particular, the GNB platform has been used for the BRIght Target Explorer (BRITE) constellation of stellar astronomy spacecraft[8], consisting of five operational satellites; the ship-tracking AISSat constellation[9], consisting of two operational satellites on-orbit and a third slated for launch; and ExactView–9, a ship-tracking mission scheduled for launch this year.

Both CanX–4 and CanX–5 are identical to each other in design. Figure 2 illustrates the CanX–4 and CanX–5 spacecraft layout, while Figure 3 and Figure 4 respectively show the two spacecraft during the vibration and thermal vacuum (TVAC) portions of their acceptance testing.

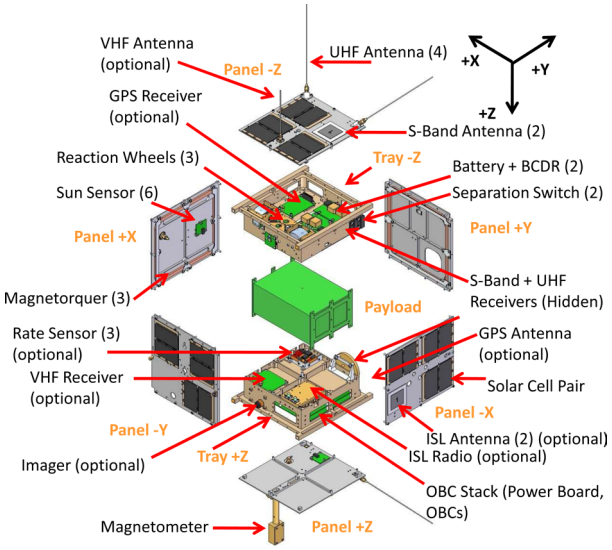

Figure 1: Exploded view of the SFL Generic Nanosatellite Bus (GNB)

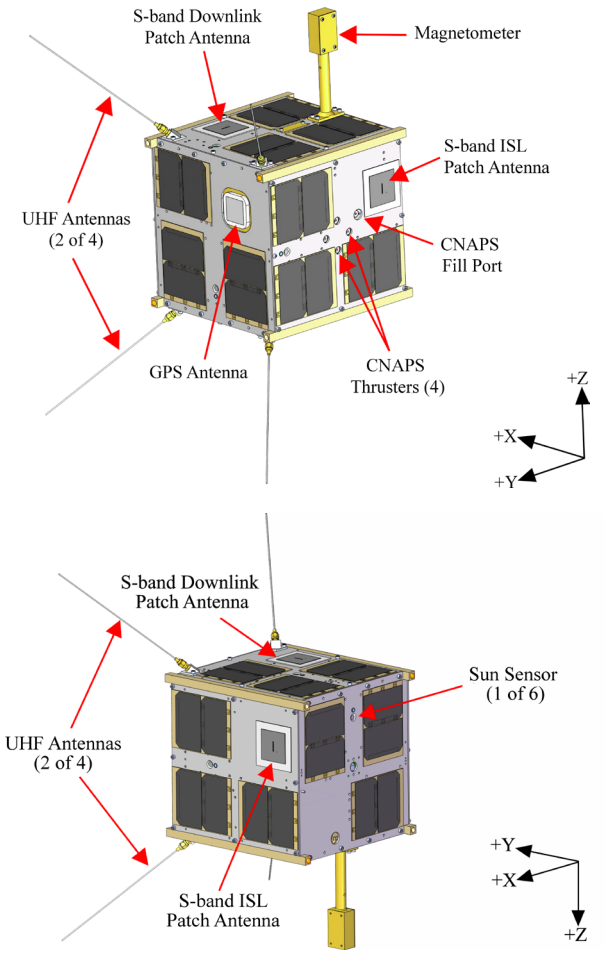

Figure 2: CanX–4 spacecraft (CanX–5 identical)

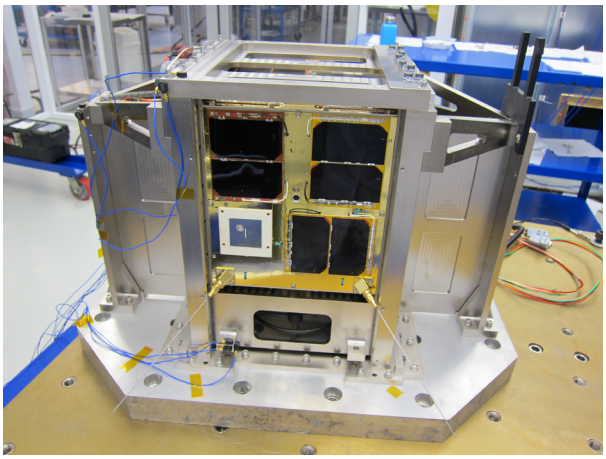

Figure 3: CanX–4 undergoing vibration testing

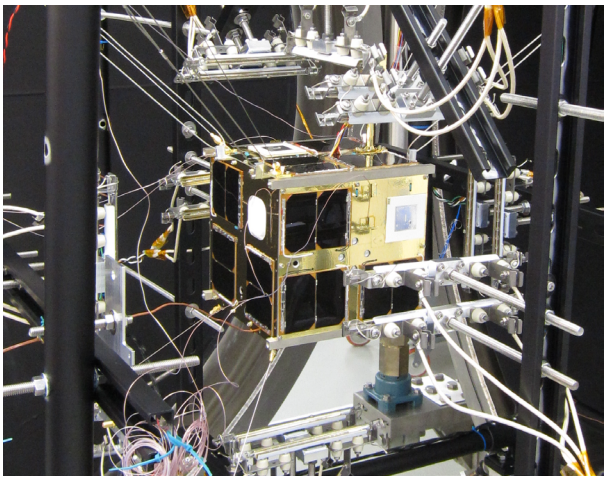

Figure 4: CanX–5 undergoing TVAC testing

For downlink, CanX–4&5 use an S-band transmitter connected to two wide-beam S-band patch antennas, mounted on opposite faces to provide near-omnidirectional coverage, with downlink speeds between 32 kbps and 256 kbps. Command uplink is implemented via a UHF receiver with a canted turnstile antenna system, also providing near omnidirectional coverage. This overall communications approach avoids so-called "death modes" in the communications system, allowing spacecraft communications in all attitudes. During autonomous formation flight, data is passed between the spacecraft using an S-band inter-satellite link (ISL), which has a demonstrated range exceeding 100 km with an omnidirectional antenna system.

The power system is a parallel-regulated direct energy transfer (DET) system, with dual parallel battery charge/discharge regulators (BCDRs) responsible for battery charging and enabling peak power tracking when required. All power is distributed centrally via a power board using solid-state switches for current consumption

monitoring and overcurrent detection and fault isolation when needed.

As with all GNB spacecraft, CanX–4 and CanX–5 each carry a suite of attitude sensors and actuators for full three-axis attitude determination and control. These include six fine sun sensors, a three-axis rate sensor, a three-axis magnetometer mounted on an external pre-deployed boom, and three sets of orthogonally mounted magnetorquers and reaction wheels. A GPS receiver and antenna are used to collect high precision information on spacecraft position.

Propulsion

The Canadian Nanosatellite Advanced Propulsion System (CNAPS) provides orbital control for orbit acquisition and phasing (drift recovery), station keeping, and formation control and reconfiguration. CNAPS is equipped with four thrusters and fueled with 260 g of liquid sulfur hexafluoride (SF_6) propellant, providing a specific impulse of 45 s and a total Δv capability of 18 m/s.

SF_6 was selected for its high storage density and vapour pressure, making the system self-pressurizing, as well as its inert and non-toxic properties, making it safe to handle and compatible with most materials. Two filters are present in the system to remove contaminants that could damage the solenoid valves, and a pressure relief valve on the storage tank prevents the possibility of an overpressure event compromising safety on the ground or the launch vehicle (Figure 5).

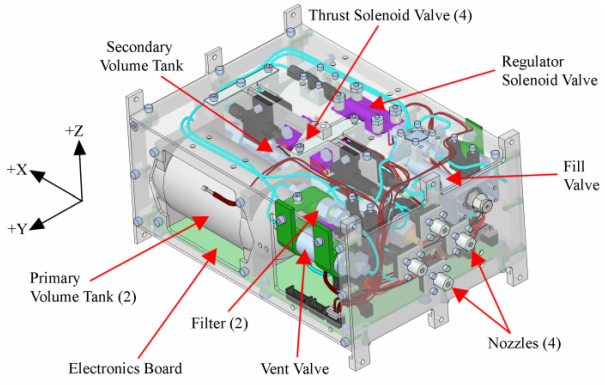

Figure 5: Interior view of CNAPS

Thrust levels range from 12.5 mN to 50 mN, depending on the chamber pressure and the number of selected thrusters. As the four nozzles are located on a single face of the spacecraft bus and offset from the centre-of-mass, thruster selection also allows the system to be used for momentum management, with the nozzle set being autonomously selected to reduce momentum build-up on the spacecraft.

Intersatellite Link

The intersatellite link (ISL) radio enables autonomous on-orbit communications between the two spacecraft. The ISL is a compact, medium-range, low-data-rate S-band radio link. Each spacecraft is equipped with a radio module (Figure 6) and two dedicated patch antennas. The ISL provides the timely and bi-directional exchange of data messages between the two spacecraft at distances up to 5 km and data rates up to 10 kbps. The maximum distance is set by estimates of the worst-case spacecraft separation distance during reconfiguration manoeuvres. In addition, this range allows for autonomous recovery of formation flight from a free-drift configuration, such as might occur if a fault interrupted nominal conditions.

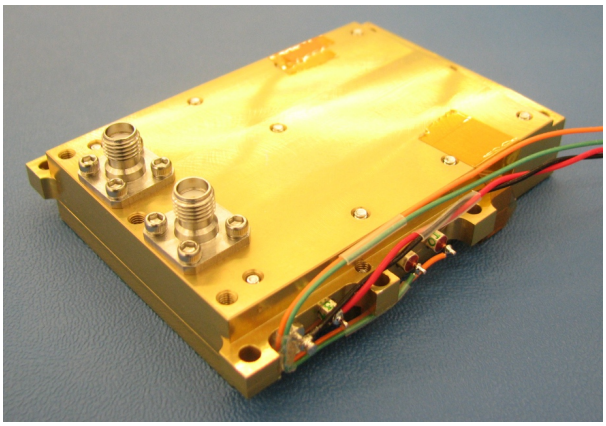

Figure 6: ISL radio module

The radio module is housed in a small enclosure which provides electromagnetic shielding, crucial to avoiding mutual interference between the ISL and the spacecraft telemetry transmitter, and substantially simplifies handling during spacecraft assembly, integration, and testing. The radio uses an RF transceiver subassembly for the transmission, modulation, demodulation, and reception of wireless data. The output of the RF transceiver is routed to a power amplifier and via a power splitter to each of the antenna ports. A baseband processor provides an interface between the spacecraft bus and the RF cores, communicating with the spacecraft payload computer using a serial link. This baseband processor also provides protocol translation and is firmware-upgradeable, allowing for the implementation of different protocol stacks.

The ISL consumes 400 mW of power when receiving and 600 mW of power during transmission. It provides 21.8 dBm of RF output power to the antennas, which emit 15.3 dBm of equivalent isotropically radiated power. With the measured antenna gains, simulations showed that a link availability of greater than 98% is achievable during formation flight, and better than 90% availability at the 5 km maximum design distance[10].

ALGORITHMS

There are three pieces of navigation and control software that help fulfill the high-level formation control requirements—the formation flying integrated onboard nanosatellite algorithm (FIONA), the relative navigation algorithm (RelNav), and the onboard attitude system software (OASYS). FIONA and RelNav run at a 5 s period on the Deputy spacecraft, while OASYS runs asynchronously at a 2 s period on both spacecraft. The primary roles of OASYS are to re-orient the spacecraft to commanded attitude targets, reverting to zenith tracking in the absence of an attitude target, and to select the thruster(s) to be used for upcoming manoeuvres. RelNav is responsible for estimating the relative orbital state of the two spacecraft using differential GPS techniques. Lastly, FIONA computes formation keeping and reconfiguration control manoeuvres and performs absolute state estimation of the Chief and Deputy orbits.

OASYS

During fine formation control, OASYS's commanded attitudes are inertial quaternions computed by FIONA on the Deputy spacecraft. The $+X$ face of the spacecraft is aligned with the target thrust direction while the $+Y$ face is constrained to be as close to zenith as possible. This attitude maximizes the number of GPS satellites in view. The target attitude computed on the Deputy is sent to the Chief via the ISL so that both spacecraft acquire the same attitude. Identical attitudes both maximize the number of common GPS satellites in view—improving relative navigation—and minimize the impact of differential perturbation forces.

Attitude determination is performed using an extended Kalman filter (EKF) operating on all available sensor data at each epoch to estimate the quaternion and angular velocity. Attitude propagation between epochs employ the quaternion kinematics and Euler's equation of rotational motion. The modeled disturbance torques include gravity gradient, magnetic control torque, wheel control torque, and thrust torque. The PID feedback control laws are formulated in terms of the Euler axis and angle error. That is, if the error quaternion is given by

$$\boldsymbol{q}_e = \begin{bmatrix} \boldsymbol{a}_e \sin(\frac{\phi_e}{2}) \\ \cos\left(\frac{\phi_e}{2}\right) \end{bmatrix}, \tag{2}$$

then here the proportional error term is $\boldsymbol{a}_e \phi_e$. This formulation was found to have faster response and settling times than the typical formulation. During long thrust periods, the assumed thrust torque is used as a feedforward term to maintain pointing accuracy. On the Chief spacecraft magnetorquers are used for wheel momentum regulation, while on the Deputy OASYS selects the set of thrust nozzles that will result in the greatest reduction in the wheel angular momentum, or the smallest increase if no reduction is possible. Magnetorquers are not used on the Deputy during formation flying to improve pointing accuracy. To improve the navigation performance in the absence of commanded target attitudes, OASYS is programmed to revert autonomously to a zenith-tracking attitude with the GPS antenna boresight.

RelNav

The relative navigation algorithm is an EKF which uses carrier phase differential GPS techniques to estimate the relative state of the Deputy with respect to the Chief as an input to the formation control laws. The concepts in RelNav's design were adapted from numerous sources[11,12,13,14,15,16] whose contributions are gratefully acknowledged. The RelNav state vector is given by

$$\boldsymbol{x} = [\Delta\boldsymbol{r}^{\mathrm{T}}, \Delta\dot{\boldsymbol{r}}^{\mathrm{T}}, \Delta b,\ \Delta N_1, \cdots, \Delta N_m]^{\mathrm{T}}, \tag{3}$$

where $\Delta\boldsymbol{r}$ is the relative position expressed in the WGS 84 Earth-centered Earth-fixed (ECEF) reference frame, $\Delta\dot{\boldsymbol{r}}$ is the relative velocity, Δb is the differential clock error, and ΔN_i is the i^{th} floating point single-difference carrier phase ambiguity. This is a dynamic state vector whose length changes with the number of GPS satellites commonly tracked by the two spacecraft. The maximum number of common satellites is 14, the number of independent channels on the GPS receiver. The relative orbit state is propagated using pseudo-relative dynamics[15,16]. One step of a fourth order Runge-Kutta integration method is used to propagate between epochs; the nominal filter step is 5 s. Filter initialization is performed using the scheme proposed by Leung[16].

At each filter update step, RelNav processes single-difference pseudorange and carrier phase measurements. During measurement evaluation the time of signal transmission from each GPS satellite is solved iteratively[12]. The GPS satellite orbits are evaluated using the latest broadcast ephemeris parameters logged from the receiver. The measurements are assumed to be uncorrelated, allowing the use of scalar measurement updates[16], which obviates the need for matrix inverses and greatly reduces computational cost.

FIONA

The formation flying integrated onboard nanosatellite algorithm (FIONA) is responsible for autonomously computing the formation reconfiguration and formation keeping control manoeuvres. FIONA implements an EKF to estimate the absolute states of both the Chief and Deputy spacecraft used to compute auxiliary control parameters—e.g. reference orbital elements—as well as to map the relative state estimated by RelNav into the

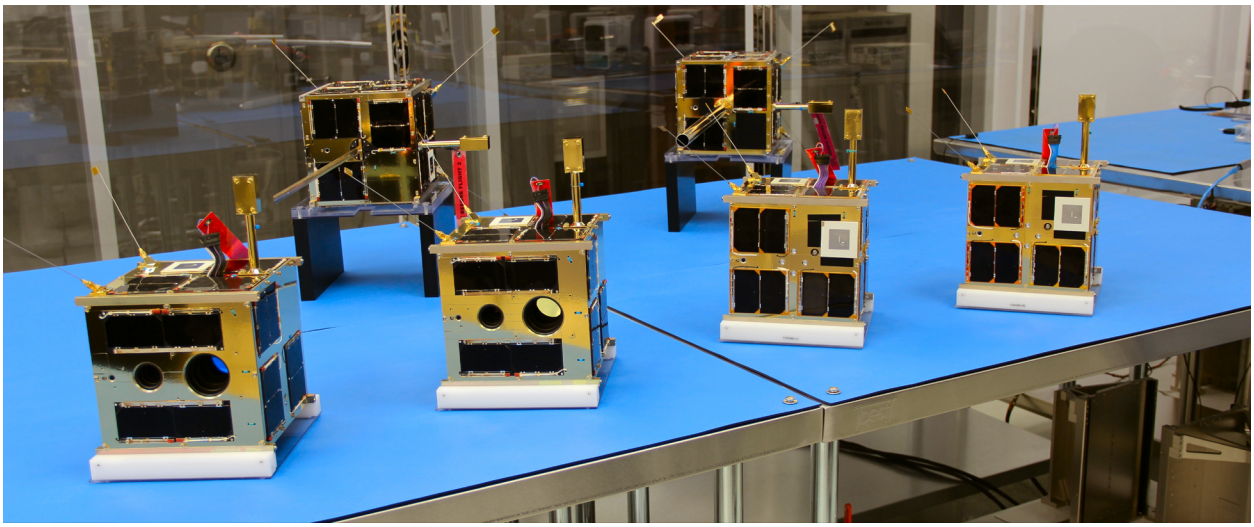

Figure 7: SFL "Summer of Spacecraft", clockwise from right: CanX-4&5, BRITE-Canada 1&2, EV9, and AISSat-2. All spacecraft (except EV9, launching Q3 2015) were flown within three weeks in Summer of 2014.

LVLH frame required for the formation control laws. The EKF is necessary to smooth the single-point position and velocity estimates coming from the GPS receiver, which suffer from a high degree of noise, especially in the velocity terms.

The formation-keeping controller is a discrete-time linear quadratic regulator (LQR) designed using the error dynamics of the HCW equations[17]. This formulation is possible since the reference trajectories are solutions to the equations of relative motion. The output of the LQR is converted to a control impulse to be applied. The nominal control time step is 75 s, of which 15 s is allotted for thrusting. In the worst case, this gives the attitude control system 60 s to perform a full 180° reorientation.

FIONA's reconfiguration algorithm identifies a set of impulsive manoeuvres which minimize an energy-like cost function subject to the relative motion constraints as described by an arbitrary state transition matrix (STM)[18]. The reconfiguration algorithm requires a start time, end time, as well as a number of thrusts. The thrusts are spaced equally throughout the time domain. After the application of each thrust in the sequence, the remaining thrusts are recomputed, effectively leading to a closed loop reconfiguration that is more robust to manoeuvring errors. In practice, the Ankersen-Yamanaka STM[19] was used since it provided the best accuracy for the least computational complexity of the STMs considered.

FIONA will only command a thrust/attitude at the start of a control time step and if the RelNav solution has been marked as "reliable", otherwise the current attitude is held. The nominal values for the minimum and maximum impulses are 7.5 mN·s and 375 mN·s, respectively. Commanded impulses greater than the maximum are set to the maximum and any values less than the minimum are set to zero. A commanded impulse of zero will not result in a new attitude command. Successive periods of no commanded thrust will thus result in an autonomous reorientation to a zenith-tracking attitude, which subsequently improves the relative navigation solution and ensures that the next commanded thrust is as accurate as possible.

LAUNCH AND EARLY OPERATIONS

Launch Campaign and the "Summer of Spacecraft"

The CanX–4&5 launch campaign spanned the majority of June 2014. At the same time, SFL was undertaking two other launch campaigns. In addition to CanX–4&5 flying with SPOT–7 on PSLV C23, SFL was concurrently integrating AISSat–2 on Soyuz-Fregat at the Baikonur CosmoDrome, as well as the BRITEs-Canada on Dnepr in Yasny.

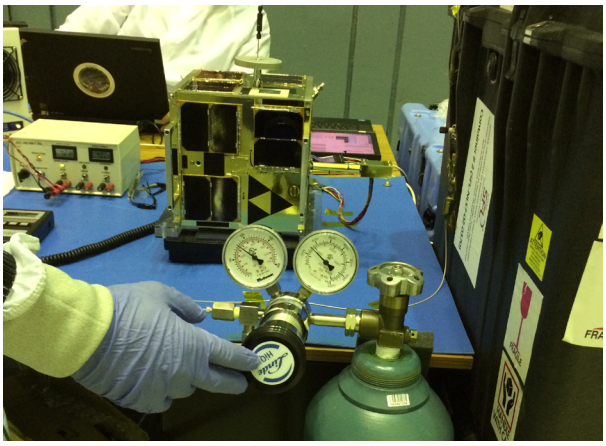

Figure 8: Fuelling of CanX–5 at SHAR SP1

Figure 9: Integrated PSLV C23 upper stage with SPOT–7 (primary, top), CanX–4 and CanX–5 (beneath SPOT–7), AISat (lower right), and VELOX-1 (not pictured) at SHAR FLP

Both CanX–4 and CanX–5 spacecraft arrived in Sriharikota, India and were unpacked at Satish Dhawan Space Centre (SHAR) during the first week of June 2014. Contrary to most larger spacecraft, both satellites were fully-tested in less than a single day, fuelled in a single morning in mid-June (Figure 8), and integrated to the PSLV Payload Launch Adaptor (PLA) over a short two-hour period on 17 June (Figure 9 and Figure 10). CanX–4 and CanX–5 were successfully launched on 30 June 2014 from Sriharikota, and deployed separately from the launch vehicle (Figure 11).

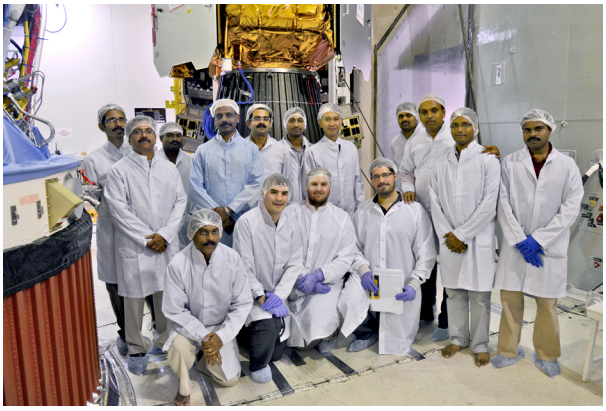

Figure 10: ISRO and SFL personnel following launch vehicle integration of CanX–4&5

Figure 11: PSLV C23 launch, 30 June 2014; image courtesy of ISRO

Commissioning Timeline and Accomplishments

Sparing no time following launch, CanX–5 was contacted on its first pass over the SFL ground station, with CanX–4 contacted on the subsequent pass. Each of these first contacts were used to download whole-orbit data (WOD), which confirmed that basic spacecraft health parameters such as solar panel currents and system temperatures were within expectations. It was generally assumed during the commissioning process that systems would work as intended, and that any experiences to the contrary would be dealt with as they

came up. The confidence necessary to take this approach was a result of the extensive ground testing of each spacecraft. Additionally, the maintenance of consistent configurations between the two spacecraft was instrumental to validating performance and facilitating meaningful comparisons. Within the first 24 hours, the GPS and ISL systems were fully commissioned. Bringing the GPS receivers online was a top priority in order to get a relative orbit determination for drift recovery purposes. The ISL, originally designed to operate to a maximum range of 5 km, was not expected to be operational by the time the spacecraft were contacted, however packets were received for three days after launch, out to a distance of about 200 km.

After verifying satellite health, the GPS receivers were turned on. At the time, the spacecraft were each tumbling at kick-off rates. Both receivers achieved a full position solution from a cold start within 13 minutes of being powered on, giving an early indication of excellent GPS receiver performance.

The first few days of attitude control system (ACS) commissioning were spent verifying the health of each spacecraft's sensor and actuator hardware. Once nominal power consumption and communications with each piece of hardware was verified, the spacecraft were placed into their passive modes. In passive mode, control torques are neither computed nor applied—only attitude determination is performed. Passive mode allows the functional state of the determination hardware to be evaluated, along with the performance and stability of the attitude EKF.

By mid-day on 4 July, four days after launch, checkout in passive mode was completed on both spacecraft. It was found that the initial body rates of each spacecraft were approximately 10°/s. This rate was determined by the attitude EKF, and correlated well with body rates determined based on the rate of change of the magnetic field in the body frame, as well as the rate of change of the panel currents in sunlight. Both spacecraft were in turn transitioned to their B-Dot control mode, employing the magnetorquers to detumble the spacecraft using the rate of change of the magnetic field in the body frame as feedback.

The body rates were rapidly reduced; approximately half an orbit was required to detumble the spacecraft. Following detumbling the focus became fully commissioning CanX–5's ACS, as this was the spacecraft chosen to perform the drift recovery manoeuvres. CanX–4 was left in passive mode following detumble while active control performance was investigated on CanX–5. On 6 July, CanX–5 was placed into a nadir-tracking attitude with its GPS antenna pointing to zenith to allow for maximum coverage of the GPS constellation. The next week and a half was spent tuning ACS control parameters and performing pointing experiments on CanX–5 in preparation for its first drift recovery thrust. On 17 July, a set of zero-impulse thrust commands with corresponding inertial target attitudes were uploaded as a dry-run for the first drift recovery thrusts to be performed the following week. Following the successful dry-run, the first drift recovery thrust was successfully executed with CanX–5 on 18 July.

In order to verify pointing and estimation during thrusting, the drift recovery impulse magnitudes were gradually increased from 65 mN·s, to 130 mN·s, to 260 mN·s, then finally 375 mN·s, the maximum configurable impulse. Estimated pointing performance and change in differential mean orbital elements during these manoeuvres were used to calibrate CNAPS. It was found that CNAPS consistently delivered approximately 20% higher impulse than observed in ground testing. This over-performance was attributed to back pressure build-up in the small vacuum chamber used for testing and correlates well with theoretical expectations. After updating the feedforward torque parameters, pointing error during maximum impulse thrusts was reduced to 4°. On 22 July, after the drift recovery campaign had begun in earnest, CanX–4 was placed into a nadir-tracking attitude. Over the next month, CanX–5 was dedicated to drift recovery thrusts, as attitude control performance was further tuned in simulations on the ground and verified on-orbit using CanX–4.

Drift Recovery and Station Keeping

The objective of the Drift Recovery and Station Keeping (DRASTK) system was to place one spacecraft directly behind the other, approximately 3 km apart, with as close to zero relative motion as possible. In mean orbital element terms, this means going from an initial state, with the spacecraft drifting under the effects of differential elements, to a final state where the elements of one spacecraft match those of the other, except for a small difference in the true anomaly. To do this, an impulsive control scheme was developed, based on Gauss' variational equations.[20]

CanX–4 and CanX–5 were mounted on to the PSLV launch vehicle using separate XPODs. The original design had the spacecraft ejected together from a single XPOD, and only separated once they had been fully commissioned and could be quickly brought in to stable relative orbits. However, launch vehicle constraints prevented this. Therefore, it became very important that at least one spacecraft become fully commissioned quickly, in order to begin arresting their relative drift. This is consistent with the Chief-Deputy formation architecture, where one spacecraft, designated the

"Chief", is defined as the reference orbit, and the second spacecraft, designated the "Deputy", is controlled relative to it. CanX–4 was assigned to be the nominal Chief and CanX–5 the Deputy.

Table 2: Differential mean orbital elements of CanX-5 to CanX-4 immediately after launch

Differential mean element	Value
Semi-major axis	-708 m
Eccentricity	-1.75×10^{-4}
Inclination	-2.32×10^{-3}°
RAAN	-1.51×10^{-3}°
Argument of perigee	55.2°
Mean anomaly	-57.6°

From GPS data post-processed on the ground, the relative mean orbital elements immediately after launch vehicle kick-off were determined and are shown in Table 2. The most important relative element from a drift recovery standpoint is the relative semi-major axis (Δa), as it defines the secular drift rate between the spacecraft. With a Δa of -708 m, the spacecraft were drifting apart at about 95 km/day.

These relative states were input to the DRASTK algorithm. The algorithm accounts for fuel spent on manoeuvres, propellant leakage over time, and the desire to maximize the number of thrusts that take place in sunlight where attitude control is more reliable than in eclipse. It also allows faster or slower trajectories to be chosen based on operational requirements.

The optimal trajectory required Δa to be changed to 306 m and Δi to be changed to 0.00129°. Inclination is changed along with semi-major axis because that allows the secular change in right ascension of the ascending node (RAAN), known as the precession of the node, to be controlled. Nodal precession is caused by the oblateness of the Earth, also known as J2, and is a function of semi-major axis and inclination.[7] Failing to correct the RAAN difference would create a large and undesirable out-of-plane motion between the spacecraft, and it is generally cheaper to correct it via a small inclination change propagated over time than to correct the RAAN alone impulsively.

Manoeuvres to put the Deputy onto the return trajectory took place 24–27 July 2014. During these manoeuvres, it was discovered that the propulsion system was performing near its theoretical maximum specific impulse, exceeding expectations by ~20%. This, combined with knowledge that drift recovery could be completed for far less than the 5 m/s that was originally budgeted, meant that a considerable amount of margin was available to use. Therefore, the decision was made to increase the speed of drift recovery such that station keeping would be entered in early September, at an additional cost of about 29 cm/s. Thus, the return trajectory was altered on 29 July to have a Δa of 720 m and Δi of 0.0030°.

On 16 August, the spacecraft reached a relative range of 315 km, from a maximum of 2300 km on 25 July (Figure 12). At this point, deceleration thrusts began, such that the spacecraft maintained a minimum separation of 3 days for safety. Control thrusts were applied every 2 days, which was a compromise between thrusting every day, which would allow slightly faster recovery, and thrusting less often which requires less operator time. Using this method, the Deputy stayed within 12 km of the reference trajectory. That error dropped to less than 2 km when the spacecraft were 15 km or closer (Figure 13). The process took about 17 days, ending on 2 September. When the final drift arresting thrust was sent on 3 September, the spacecraft were within 50 m of their nominal parking positions with nearly zero residual relative orbital elements (Table 3).

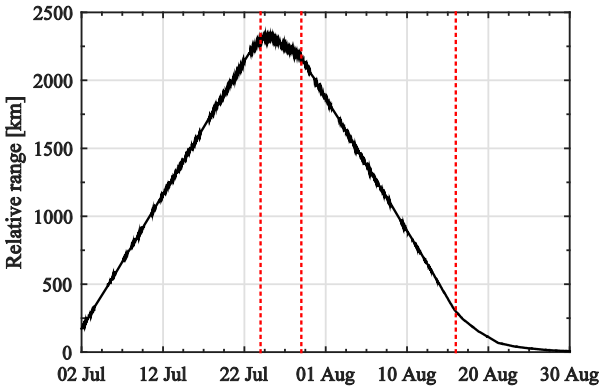

Figure 12: Relative range of the two spacecraft and trajectory transitions during drift recovery phase

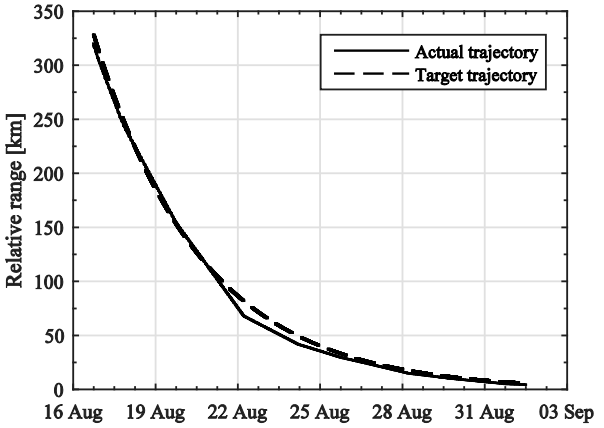

Figure 13: Actual and targeted return trajectory during deceleration phase

Table 3: Differential mean orbital elements of CanX–5 to CanX–4 after completing drift recovery

Differential mean element	Value
Semi-major axis	0.5 m
Eccentricity	8.0×10^{-7}
Inclination	1.0×10^{-6}°
RAAN	1.3×10^{-6}°
Argument of perigee	0.014°
Mean anomaly	0.009°
Range	2.95 km

Total Δv expended in manoeuvres during drift recovery is predicted to have been 2.032 m/s, based on the best estimates of on-orbit thruster performance. Based on simulations done on the ground, assuming no attitude or navigational errors, the minimum cost to perform these manoeuvres would be 1.922 m/s. The error, 5.71%, is well within expectations from simulations, where the mean error was found to be 5.8% with a standard deviation of 2.7%.An additional 0.813 m/s was spent on station keeping manoeuvres after and between each of the four formations. The majority of this fuel was used putting the spacecraft into passively safe relative states immediately upon exiting the PCO formations, when the risk of a collision was highest.[20]

GPS Performance

From very early on it was found that the GPS receivers on both spacecraft were performing exceedingly well. The first position fix from CanX–5 was recorded on 30 June 2014 at 14:19:44 UTC, approximately 13 minutes after being powered on for the first time. Remarkably, this first lock was achieved in the absence of attitude control while the spacecraft was tumbling at 10°/s. Similarly, the first position fix from CanX–4 was recorded on 30 June 2015 at 15:54:44 UTC, again 13 minutes from being powered up and tumbling at the same rate. These cold start times were in fact better than those obtained on the ground in GPS signal simulator testing with non-tumbling spacecraft.

To better characterize the GPS system performance, carrier-to-noise-density ratio (C/N_0) as reported by the receiver was recorded at a one minute cadence over a span of five orbits, along with high rate attitude data. Using the known satellite geometry, the C/N_0 was expressed as a function of the GPS satellite elevation with respect to the GPS antenna boresight. The measurements were binned based on their angle from boresight, and within each bin, the mean C/N_0 was computed (Figure 14). It is evident that the on-orbit results are much better than those assumed during preparation for the mission in hardware-in-the-loop tests. With these results, the GPS receivers were considered commissioned and ready to be put to the test during the more demanding portions of the mission.

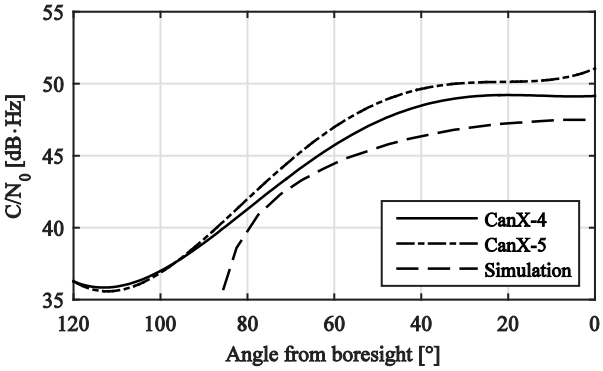

Figure 14: C/N_0 as a function of elevation with respect to GPS antenna boresight

The accuracy of the GPS-reported solutions were also assessed by comparing them to post-processed estimates on the ground. The post-processed estimates were obtained from an EKF filter/smoother operating on independently obtained single-point positions from edited pseudorange data and single-point velocities from Doppler data. Example position and velocity residuals obtained from this process are shown in Figure 15 and Figure 16 respectively.

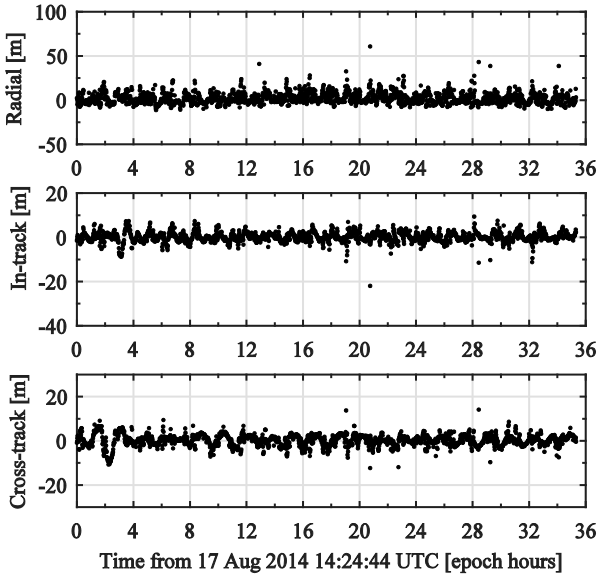

Figure 15: GPS position residuals in the RIC frame

Generally, the position solutions were accurate to 10 m in each axis with occasional spikes exceeding 30 m. These spikes were caused by low-elevation satellites being used in the single-point solution. It was also found that the radial solution exhibited a bias of 2 m, which was expected based on the geometric distribution of the GPS satellites. Generally, the velocity solutions were quite poor, being accurate to only 0.2 m/s in each axis, and exhibiting large error spikes up to 8 m/s. The cause of these spikes was not investigated.

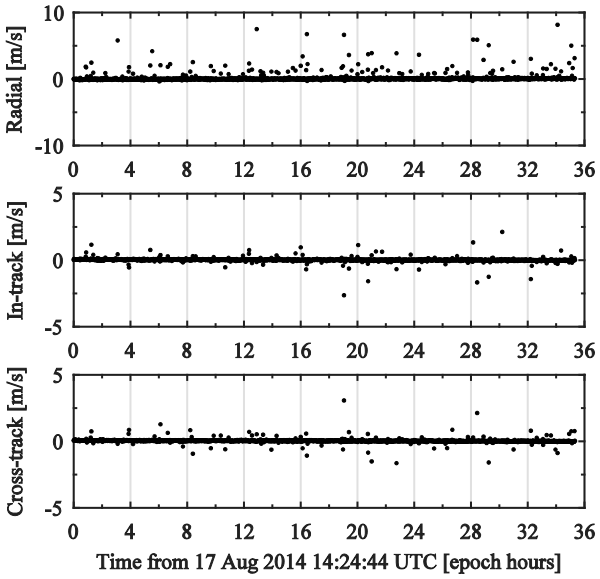

Figure 16: GPS velocity residuals in the RIC frame

ISL Performance

Within 24 hours of first contact, the ISLs on both spacecraft were brought online. The first successful link was established at 01 July 2014 02:55:52 UTC at a range of 85 km while the spacecraft were still tumbling. The ISLs operate as a transparent network bridge between the spacecraft, exchanging attitude and GPS data. They were left operating in this mode while the spacecraft continued to separate during commissioning.

Once the attitude control systems were commissioned, the spacecraft were oriented in a zenith-tracking mode with the ISL antenna boresights aligned with the velocity direction, maximizing the system gain between the spacecraft. The last successful link during the outbound phase of drift recovery was at 01 July 2014 23:21:52 UTC at a maximum range of 170 km. During the return phase, when the antenna boresights were aligned, the link was established at a range of 200 km and was reliable—i.e. greater than 90% availability—once the spacecraft were within 100 km range of each other. Throughout the formation flying experiments, in which the spacecraft were well under the 5 km design limit, the ISL exhibited near 100% system link availability (Figure 17). The total amount of data exchanged between the two spacecraft over the course of the nominal mission was 1.19 GiB.

FORMATION CONTROL RESULTS

Before discussing the formation control results, it is worth summarizing the typical experiment planning methodology. The first step was to download GPS data and use DRASTK to compute a set of thrusts to bring the spacecraft to within roughly 1000 m of the target

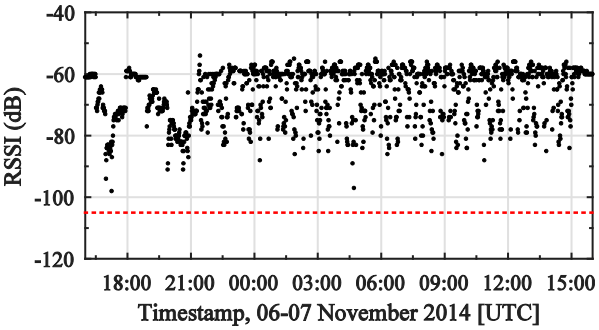

Figure 17: ISL system RSSI during 1000 m ATO

formation in a passively safe relative orbit. Next, offline formation control simulations were performed using the predicted relative orbit as the initial condition to establish reconfiguration start and end times, along with the expected fuel consumption. The reconfigurations were designed to begin near the start of a morning pass block—the two to four communications windows that occur for CanX–4&5 each morning over the SFL ground station—with an overall duration of three or four orbits so that the early reconfiguration progress could be monitored during the remainder of the morning passes.

All formations were held for 11 orbits and the end of the 11th orbit was designed to take place before or during the next pass block. This was done so that, if required, manoeuvres to safe the relative orbits could be performed as soon after the end of the formation as possible. Typically, at least two days were needed to download the large volume of payload data collected. During this time, the spacecraft were placed into safe relative orbits prior to commencing the next experiment.

Special considerations were required for the PCOs, since this formation can result in a collision within a few orbits following loss of formation control. During experiment planning, a set of contingency thrusts (one set for each ground contact during the experiment) were computed in DRASTK and prepared for upload in case it was found that the spacecraft had fallen out of formation. These thrusts were designed to restore the 90° phase offset between the radial and cross-track motion to ensure passive safety of the formation. Fortunately, the contingency thrusts were never required.

Table 4: Timeline of formation flying experiments

Date	Formation	Notes
01 Oct	1000 m ATO	Navigation errors larger than desired due to attitude targeting between manoeuvres
15 Oct	500 m ATO	Formation control requirements met
21 Oct	100 m PCO	Formation control requirements met
02 Nov	50 m PCO	Formation control requirements met
06 Nov	1000 m ATO	Formation control requirements met

The timeline for the formation control experiments performed is shown in Table 4. The first formation attempt was the 1000 m ATO. In this attempt the formation was established and maintained for the required 10-orbit period; however, the control error was sub-metre only 88% of the time, instead of the 95.45% requirement. The ultimate cause was found to be poor navigation performance due to FIONA commanding target attitudes even if the desired impulse was naught. This led to the GPS antennas often pointing away from zenith, resulting in fewer commonly tracked satellites with acceptable C/N_0 and thus less reliable solutions. The higher number of unreliable solutions resulted in less control thrusts and thus more excursions outside the desired control window. Even so, the maximum control error observed during this experiment was only 2.25 m, which was still an excellent result.

After analyzing the first experiment's results and identifying the cause for the degraded navigation performance, a new software upload was performed prior to attempting the 500 m ATO. With the improvements in the attitude targeting, the 500 m ATO was a complete success. As shown in Figure 18, after the initial convergence period following the end of the reconfiguration maneuver, the control error remained sub-metre for the duration of the experiment. The periods of time where the control error is increasing correspond to times where the commanded impulse was below the minimum impulse bit. The applied impulses for this experiment are shown in Figure 19. The first seven thrusts correspond to the reconfiguration manoeuvre. Following this, three more manoeuvres are required before settling into a steady state of operation. The mean time between control thrusts in this experiment was 8 minutes and 40 seconds—far less frequent than the originally anticipated control period of 75 s. The actual fuel consumption was 1.6 cm/s/orbit—just under the expected value of 1.7 cm/s/orbit based on hardware-in-the-loop tests on the ground.

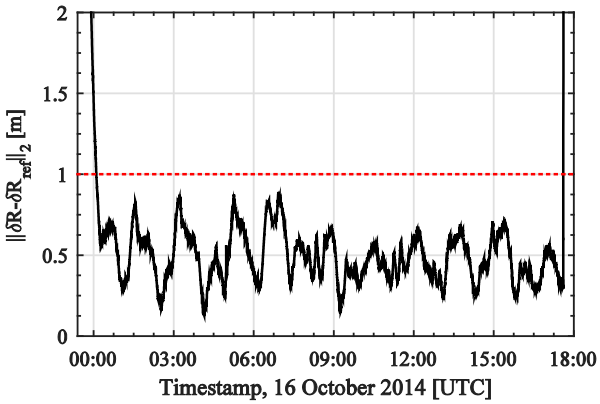

Figure 18: Position control error for the 500 m ATO

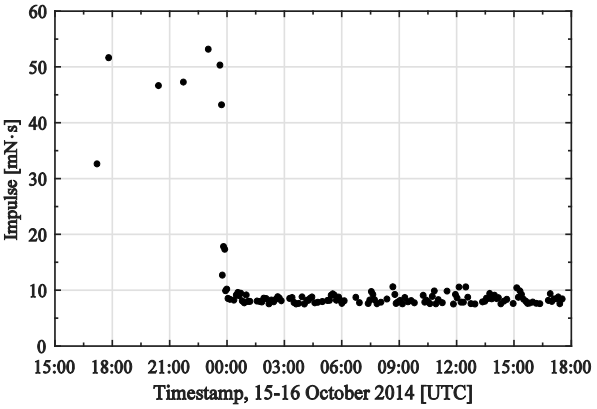

Figure 19: Applied manoeuvres for the 500 m ATO

Having succeeded with the ATOs, the PCO experiments were started a few days later. The reconfiguration error was larger than expected, at 14 m. The fuel consumption was also 5 cm/s larger than expected based on pre-experiment planning. Although the exact cause is not known, the most likely cause of this is an error in the magnitude/direction of one of the computed thrusts due to a slightly degraded relative navigation solution. Despite this, the LQR was successful at reducing the control error from 14 m to 1 m over the first 45 minutes. Once converged, the formation control error remained well below 1 m (Figure 20).

The sequence of applied impulses for this formation is shown in Figure 21, where the periods of convergence and steady state operation are evident. Not accounting for the additional fuel used during convergence, the steady state fuel consumption was 1.15 cm/s/orbit, roughly 0.15 cm/s/orbit above the predicted value.

The 50 m PCO was attempted 9 days following the 100 m PCO. Operationally this was the most dangerous of all the formations due to the proximity of the spacecraft and the fact that loss of formation control could easily lead to collision. However, by this point in time the team had a high degree of confidence in the system given the previous successes. As shown in Figure 22, the initial reconfiguration error was less than 2 m. At this point, the LQR took over and maintained a sub-metre control error for the duration of the formation. The mean fuel consumption was roughly 1.3 cm/s/orbit—less than half the expected value based on pre-flight simulations. This is attributed to the high accuracy of the relative navigation solution—in particular the relative velocity.

Following the successful completion of the 50 m PCO, it was decided to revisit the 1000 m ATO to demonstrate unequivocally that high-level mission requirements could be met in every formation. The control error

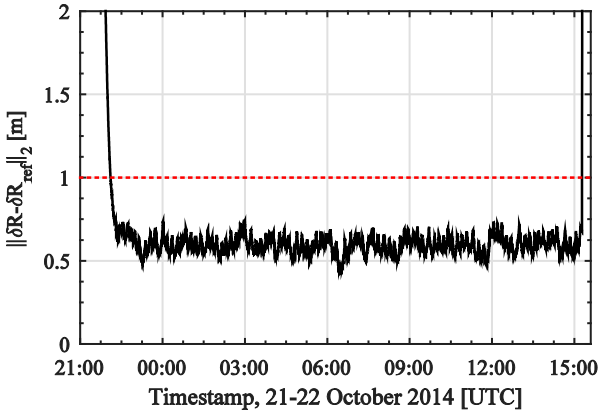

Figure 20: Position control error for the 100 m PCO

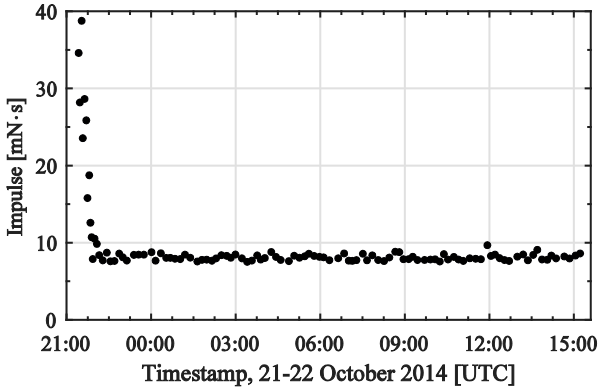

Figure 21: Applied manoeuvres for the 100 m PCO

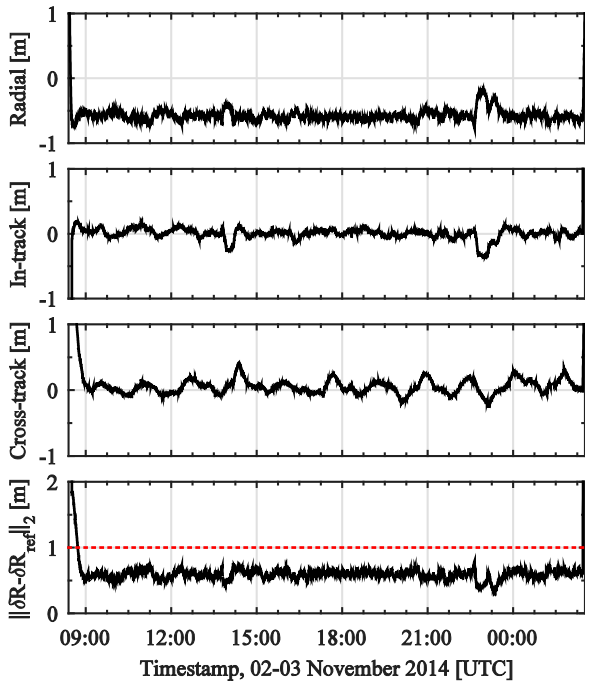

Figure 22: Control errors for the 50 m PCO

following reconfigurations was the largest seen in the mission so far—35 m in relative position and 4 cm/s in relative velocity. This occurred despite no apparent relative navigation or thrust application issues. Fortunately, this was still inside the stability boundary for the LQR and the control error was successfully reduced to the required level over the course of one orbit.

As shown in Figure 24, there was a large fuel penalty associated with using the LQR to reduce the control error by such an extent—almost 26 cm/s. However, once the control converged the fuel consumption came to a steady state value of roughly 3.4 cm/s/orbit, just under the expected value of 3.65 cm/s/orbit.

As shown in Figure 23, the control error following the convergence remained sub-metre for the duration of the experiment. Note that the apparent sudden changes in relative position are in fact gradual—the data points in between are removed since they were flagged as unreliable. The control error grows during these navigation outages since no thrusts are performed.

Table 5: Summary of formation control results

Formation	$\Delta v_{expected}$ [cm/s/orbit]	Δv_{actual} [cm/s/orbit]	Δr_{actual} 3D-RMS [m]	Δr_{actual} 3D-RMS [m]
ATO 1000	3.65	5.55	0.590	0.453
ATO 500	1.71	1.62	0.345	0.513
PCO 100	0.99	1.63	0.517	0.602
PCO 50	3.07	1.27	0.554	0.594

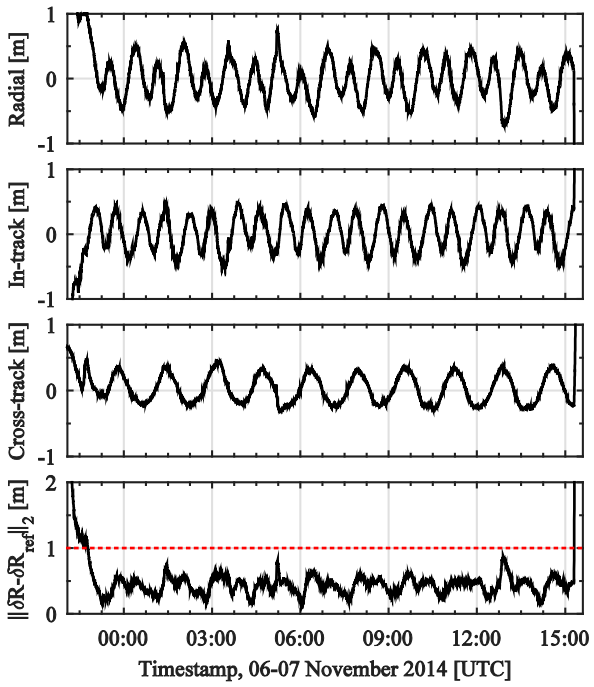

Figure 23: Control errors for the 2nd 1000 m ATO

A performance summary for the fuel consumption and formation control error for all formation flying experiments is shown in Table 5. As mentioned previously, the discrepancy between the actual and expected fuel consumption is due to the initial convergence period of the LQR. During steady state operation, the fuel consumption was close to the expected value in all cases. The 3D-RMS control error was well within the 1 m, 2σ requirement in all cases.

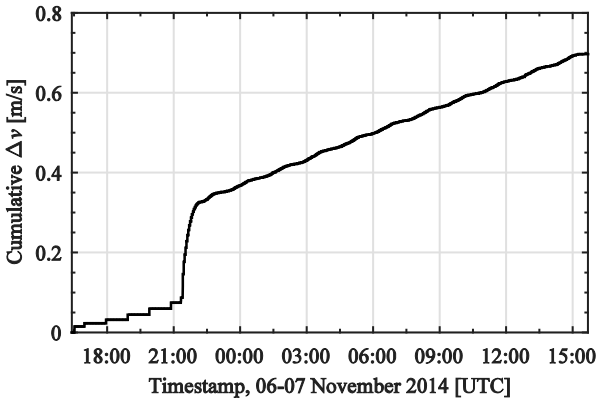

Figure 24: Fuel usage for the 2nd 1000 m ATO

An example of the RelNav performance following commissioning is shown in Figure 25. Here the measurement residuals during the 50 m PCO formation flying experiment are evaluated using the on-orbit solution. The GPS satellite orbits are computed using the broadcast ephemeris parameters since GPS orbit errors do not contribute significantly to the overall error as a result of the single-difference measurements.

For the most part, the residuals meet the expected result of a zero-mean Gaussian distribution, which indicates that the EKF is operating correctly. It can also be seen that there are several periods where the residuals show a larger spread. These periods are typically due to dynamic events—rapid reorientations where many satellites are added and removed from the state vector, as well as thrusts where the change in spacecraft velocity is instantaneous.

It is also common to see a period of large residuals following a period of open-loop propagation caused by too few commonly tracked satellites, such as at the start and end of the time span. Examination of the solution at these epochs reveals that the relative position and velocity estimates remain consistent and smooth and it is the differential clock bias that most affects the residuals. This is likely due to the fact that the GPS receivers automatically steer their clocks to GPS time so that the differential clock bias cannot be predicted in the absence of EKF updates.

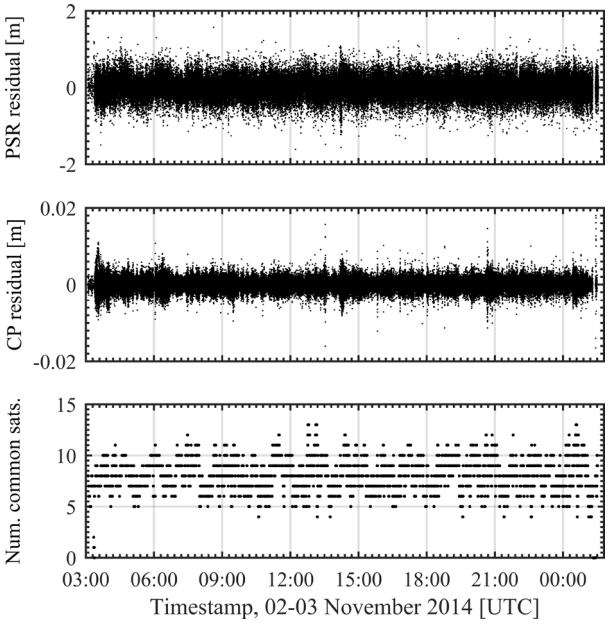

Figure 25: RelNav measurement residuals for the 50 m PCO formation flying experiment

CONCLUSIONS AND FUTURE WORK

In only four months following launch, the CanX–4 and CanX–5 dual satellite formation flying mission was accomplished, ahead of schedule and with all mission objectives met. This exciting mission has broken new ground in the capabilities of nanosatellite formation flying performance—techniques that are entirely portable to larger satellites and will enable much higher-performance missions in turn.

CanX–4 and CanX–5 have pushed the boundary of what can be achieved with nanosatellites. The technology and algorithms demonstrated on CanX–4&5 open a wide range of potential missions and applications, ranging from on-orbit inspection and repair, to sparse aperture sensing, interferometry, and ground moving target indication.

Meanwhile, both satellites continue to perform exceptionally well in orbit, with a large fraction of their propellant remaining. At the time of this writing, both spacecraft are approaching one year in space, having concluded their nominal mission.

ACKNOWLEDGEMENTS

The authors wish to acknowledge the CanX–4&5 formation flying mission funding sponsors: NSERC, DRDC-Ottawa, CSA, MDA, and Ontario Centres of Excellence. Without their valued contributions, development of this mission would not have been possible.

REFERENCES

1. Petrov, G.I., Conquest of Outer Space in the USSR: Official Announcements by Tass and Material Published in the National Press from October 1967 to 1970, Moscow, 1971.
2. Godwin, R., Gemini 7 – The NASA Mission Reports, Collector's Guide Publishing Inc., Burlington ON, 2002.
3. "PRISMA (Prototype Research Instruments and Space Mission Technology Advancement)," https://directory.eoportal.org/web/eoportal/satellite-missions/p/prisma-prototype, accessed 4 December 2014.
4. Clark, S., "French Sun Satellite and Swedish Experiment Blast Off on Russian Rocket," http://www.space.com/8608-french-sun-satellite-swedish-experiment-blast-russian-rocket.html, accessed 20 January 2015.
5. Sarda, K. et al., "Canadian Advanced Nanospace Experiment 2 Orbit Operations: Two Years of Pushing the Nanosatellite Performance Envelope," Proceedings of the European Space Agency Small Satellite Systems and Services Symposium, Funchal, 2010.
6. Bandyopadhyay, S. et al., "A Review of Impending Small Satellite Formation Flying Missions," Proceedings of the 53rd AIAA Aerospace Sciences Meeting, Kissimmee FL, 2015.
7. Schaub, H. and J.L. Junkins, Analytical Mechanics of Space Systems, American Institute of Aeronautics and Astronautics, 2009.
8. Grant, C. et al., "On-orbit performance of the BRITE nanosatellite astronomy constellation," Proceedings of the 65th International Astronautical Congress, Toronto ON, 2014.
9. Helleren, Ø. et al., "AISSat–1 – 2 Years of Service," Proceedings of the European Space Agency Small Satellite Systems and Services Symposium, Portorož, Slovenia, 2012.
10. Armitage, S. et al., "The CanX–4&5 nanosatellite mission and technologies enabling formation flight," Proceedings of the 7th International Workshop on Satellite Constellations and Formation Flight, Lisbon, Portugal, 2013.
11. Marji, Q., "Precise Relative Navigation for Satellite Formation Flying Using GPS," MASc thesis, University of Calgary, Calgary AB, 2008.
12. Busse, F.D., "Precise formation-state estimation in low Earth orbit using carrier differential GPS," PhD thesis, Stanford University, Stanford CA, 2003.
13. Ebinuma, T., "Precision spacecraft rendezvous using GPS: an integrated hardware approach," PhD thesis, University of Texas at Austin, Austin TX, 2001.
14. Montenbruck, O. et al., "A real-time kinematic GPS sensor for spacecraft relative navigation," Journal of Aerospace Science and Technology, vol. 6, 2002.
15. Kroes, R., "Precise relative positioning of formation flying spacecraft using GPS," Netherlands Geodetic Commission, No. 61, 2006.
16. Leung, S. and O. Montenbruck, "Real-time navigation of formation-flying spacecraft using GPS measurements," Journal of Guidance, Control, and Dynamics, vol. 28, No. 2, March-April 2005.
17. Pluym, J.P. and C.J. Damaren, "Dynamics and Control of Spacecraft Formation Flying: Reference Orbit Selection and Feedback Control," Proceedings of the 13th Canadian Astronautics Conference, Montreal QC, 2006.
18. Roth, N.H. and C.J. Damaren, "Computationally Efficient State-Transition Matrix Based Multiple-Thrust Satellite Formation Reconfigurations," Proceedings of the 15th Canadian Astronautics Conference, Toronto ON, 2010.
19. Yamanaka, K. and F. Ankersen, "New state transition matrix for relative motion on an arbitrary elliptical orbit," Journal of Guidance, Control, and Dynamics, vol. 25, No. 1, January-February 2002.
20. Newman, J.Z., "Drift Recovery and Station Keeping for the CanX–4 & CanX–5 Nanosatellite Formation Flying Mission", MASc thesis, University of Toronto, Toronto ON, 2015.